Case Studies in Neuroscience: The electrophysiology of a human obsession in nucleus accumbens

Kai J. Miller[1,4], Thomas Prieto[2], Nolan R. Williams[3]*, Casey H. Halpern[1]*
Departments of Neurosurgery[1], Neurology[2], and Psychiatry[3], Stanford University;
Department of Neurological Surgery[4], Mayo Clinic; *Equal contribution
Correspondence: miller.kai@mayo.edu (KJM) and chalpern@stanford.edu (CHH)

Abstract:
Microelectrode recordings were performed during awake deep brain stimulation surgery for obsessive-compulsive disorder, revealing robust brain oscillations that were plainly visible throughout the ventral striatum. There was an elegant topological correspondence between each oscillation and the underlying brain anatomy, most prominently a ~35Hz gamma-oscillation specific to the nucleus accumbens. Direct provocation of the patient's contamination obsession modulated both firing rate and gamma-oscillation amplitude within the nucleus accumbens.

Introduction:
Have you ever gone back into your house shortly after leaving to make sure the oven was turned off, despite remembering turning it off? Have you then had the urge to check it yet again? These transient motivations are a normal part of the human experience that reinforce patterned behavior, and most of us can suppress them when they contradict what we know to be reasonable. But this ability to suppress is dysfunctional in those with obsessive-compulsive disorder (OCD), a neuropsychiatric disease characterized by repetitive physical or mental acts (compulsions) directed toward unwanted persistent images, thoughts, or impulses (obsessions) (Westphal 1877). The execution of compulsions consumes the time and effort of individuals to the degree that they dramatically interrupt personal and professional activities (American Psychiatric Association 2013). Standard treatment is a combination of systematic exposure to the objects of obsession during cognitive behavioral therapy and medical intervention (Grant 2014).

Beginning 15 years ago, deep brain stimulation (DBS) emerged as a therapy for patients who fail the most aggressive standard treatment (Sturm et al. 2003). As a region of confluent cortical, striatal and thalamic projections, the region of the nucleus accumbens (NAc) was felt to be an ideal initial target for DBS. Long-term studies of therapeutic outcome have substantiated its' efficacy in many patients (Alonso et al. 2015; Fayad et al. 2016; Sheth et al. 2013). However, NAc DBS does not help some patients (Mian et al. 2010), and this can likely be attributed to variability in electrode positioning and individuals' functional anatomy. Variable response DBS for other diseases is partially mitigated by performing electrode implantation awake, making microelectrode recordings to identify neuronal populations whose activity correlates with disease-related tasks (e.g. limb movement in Parkinson's disease) (Romanelli et al. 2004). This strategy had remained unrealized for OCD until a patient of ours with a particular contamination obsession underwent awake NAc-DBS surgery. The provocable nature of his disease allowed for electrophysiological characterization of the fundamental processes that underlie obsessive thoughts.

Downloaded from www.physiology.org/journal/jn at Auburn Univ Auburn (131.204.073.184) on April 25, 2019.

Methods:

All recorded data, as well as analysis code in MATLAB format are available at: https://searchworks.stanford.edu/view/xf387wq3868 (open "kjm_NAc_OCD_Read_Me.pdf" at this URL for a complete description). There is also a supplement with methodological illustration and some minor additional results at the same URL, in the file "kjm_NAc_OCD_Supplemental.pdf".

Patient and surgical implantation: A 64-year-old male patient with intractable obsessive-compulsive disorder, refractory to all medications, presented for bilateral deep brain stimulation electrode (DBS) implantation of the ventral capsule/ventral striatum, a region that includes the nucleus accumbens. His disease centered on cleanliness and bathroom-related activities, particularly brushing his teeth, causing marked impairment in his ability to carry out his normal activities of daily life. The patient consented to participate in a research protocol during the awake surgery for implantation of these leads. Stanford's internal review board approved the study and the consent process (IRB #33146). Stereotactic targeting and alignment to the left nucleus accumbens was performed with the NexFrame and Stealth S7 system (Medtronic, Minneapolis, MN). A cannula was stereotactically passed from the middle frontal gyrus to the ventro-medial internal capsule aligned to nucleus accumbens in-plane with the anterior commissure (Figure 1-1). From the tip of the cannula, a microelectrode (0.5-1 MΩ platinum–iridium; FHC, Bowdoin, ME) was advanced 20mm to a target in the ventral nucleus accumbens (Figure 1-1). The target location for the stereotactic placement in the AC-PC coordinate system was at x = 6.0mm, y = 15.1mm, z = −6.6mm, with a trajectory of 34.2° from the midsagittal plane and 60.3° from the axial plane. With prolonged clinical stimulation at the border of the accumbens/commissure (Medtronic 3391 electrode spanning 7-10mm above target in figure 1), the patient achieved a 30% reduction in Yale-Brown obsessive-compulsive scale. The Medtronic 3391 lead cleared for humanitarian exemption contains 3mm leads separated by 4mm. Because of the large 3mm size of these leads, they cannot delineate NAc subregions. Likely for this reason, widespread stimulation throughout the NAc does not always provide optimal therapy, and a more dorsal stimulation program is often employed (Alonso et al. 2015).

Signal analysis: Raw voltage, $V^0(t)$, was measured from the microelectrode, referenced to the cannula, and sampled at 50 kHz using a Guideline 3000 microelectrode recording system (Axon Instruments) (gain, 10,000; band-pass filtered from 1 Hz to 10 kHz), passed through a CyberAmp 380 amplifier/filter (Axon Instruments, Foster City, CA) (band-pass filtered from 1 Hz to 6 kHz), and sampled at 50,000 samples per s using a data acquisition interface (Power1401) and Spike software (version 2.7, Cambridge Electronic Design, Cambridge, England). Although previous studies were able to extract meaningful measurements of phase below 4Hz (Wu et al. 2018), there was significant signal amplitude attenuation in this range, so we have limited our exploration in this study to frequencies above 4Hz.

A number of steps were employed to isolate spikes from the raw voltage trace (illustrated in the online methodological supplement):

- First, the raw voltage trace was high-pass filtered at 300Hz, $V^0(t) \xrightarrow[300Hz]{} \hat{V}(\mathrm{t})$ A linear threshold was then visually fit to the filtered voltage trace at each location to capture characteristic action potential voltage deflections.
- Seven millisecond windows of data were obtained surrounding the sample of furthest excursion from baseline for each action potential deflection, τ_q, from 2ms prior to 5ms

Downloaded from www.physiology.org/journal/jn at Auburn Univ Auburn (131.204.073.184) on April 25, 2019.

after (e.g. $\hat{V}_q(t') = \hat{V}(\text{t-}\tau_q)$, where -2ms $\leq t' \leq$5ms). The average of these windows gives the characteristic action potential shape.

- These data windows surrounding action potential times were then decomposed with a principal component approach. A singular value decomposition is used to determine the eigenvalues λ_k and eigenvectors $\overrightarrow{e_k}$ of the correlation matrix: $C(t', t'') = \sum_q \hat{V}_q(t')\hat{V}_q(t'')$. Note that the baseline is, in effect, subtracted off of each window as a byproduct of the high-pass filtering. These eigenvectors, $C\overrightarrow{e_k} = \lambda_k \overrightarrow{e_k}$, reveal characteristic shapes in the temporal shape of the action potential that vary orthogonally, and are ordered by magnitude of corresponding eigenvalue: $\lambda_1 > \lambda_2 > \cdots > \lambda_T$ (where $T \equiv$ number of timepoints in -2ms to 5ms interval). If we define the rotation matrix $A(k,t) = (\overrightarrow{e_1}, \overrightarrow{e_2}, \ldots, \overrightarrow{e_T})$, then the projection, $W(k,q)$, of each individual spike in the ensemble into the new eigenvector space is: $W(k,q) = \sum_{t'} A(k,t')\hat{V}_q(t')$. The inverse rotation matrix A^{-1} (where $A^{-1}A = \hat{I}$) allows us to remove the weighted spike components (the first 3 eigenvectors) surrounding spike at time τ_q from the raw voltage timeseries, leaving the local field potential (LFP): $V(\text{t'+}\tau_q) = V^0(\text{t'+}\tau_q) - \sum_{k=1,2,3} A^{-1}(t', k)W(k,q)$.

From this LFP, oscillations were characterized as follows:

- Power spectral densities (PSDs) were calculated using Welch's averaged periodogram method, with 1s windows, using a Hann window, stepping through $V(\text{t})$ in 250ms intervals (Figure 1). Peaks in the PSDs were visually apparent above a $1/f$ background shape, centered at 7Hz (theta), 9Hz (alpha), 25Hz (beta), and 36Hz (gamma).
- Rhythm amplitudes were calculated by band-passing the local field potential, $V(\text{t})$, using a 3rd order Butterworth filter for a specified frequency range, F, to obtain the "band-limited" potential, $V(\text{F,t})$. A complex analytic signal, $\tilde{V}(\text{F,t}) = V(\text{F,t}) + iV^{IM}(\text{F,t})$was constructed using the Hilbert transform, which can also be expressed in polar notation as $\tilde{V}(\text{F,t}) = r(\text{F,t})e^{i\phi(F,t)}$. In this study, the alpha range is $F \rightarrow$8-10Hz, and the gamma range is $F \rightarrow$31-39Hz.

Anatomic localization: As illustrated in Figure 1-2, microelectrode recording position was determined by fusion of the post-surgical CT to the pre-surgical MRI, using a normalized mutual information approach, and reslicing in-plane with the DBS shank while preserving midline symmetry. Then the intraoperative microelectrode recording positions were inferred from the corresponding post-implantation DBS electrode lead positions (where the terminal lead was at the target position). Grey-matter nulled MR, white-matter nulled MR, and T1-post gadolinium contrasted were overlaid, so underlying ventral striatal anatomic structures could be clearly delineated.

Compulsion provocation: A simple provocation test was designed based on a self-reported fear known to trigger his compulsive full body cleaning. After a brief baseline period, a psychiatrist at the bedside (N.W.) handed the patient a toothbrush, telling him first to bring it to his face, and then told to "imagine brushing your teeth with this dirty toothbrush". The toothbrush was then taken back from the patient, and, as a control, the patient was then instructed to bring his hand back to his face without the toothbrush (Figure 2, Supplemental video). This toothbrush provocation testing was performed twice, once each at 3mm and 1mm above target, where actively spiking neurons had been identified. Spike rate counts and average oscillation amplitudes of $r(\text{F,t})$ were calculated in one-second blocks (block size chosen arbitrarily) to calculate statistical significance during the task (as shown in figure 2).

Downloaded from www.physiology.org/journal/jn at Auburn Univ Auburn (131.204.073.184) on April 25, 2019.

Results:

A map of human brain oscillations in the ventral capsule / ventral striatal region: Field potentials measured were measured at every millimeter from the opening of a stereotactic guidance cannula to the NAc target 2cm below (Figure 1). The raw potential traces showed visually apparent oscillations, plainly reflected by peaks in the power spectral densities (PSD). When these PSDs are viewed alongside one another, a clear topological relationship between oscillatory frequency and brain anatomy emerges:

- A robust 35Hz-centered gamma oscillation ($h\gamma_{35}$) was found specifically in the NAc and nowhere else. Based upon comparison with recent human segmentations using diffusion tractography (Baliki et al. 2013), our NAc recordings are most likely in the shell subregion.
- 7Hz-centered theta oscillations extended throughout the recorded portion of the anterior limb of the internal capsule (ALIC), including where capsular fibers were co-localized with the globus pallidus (GP) and the bed nucleus of the stria terminalis (BNST).
- 9Hz-centered alpha oscillations were present throughout all structures except for the ALIC.
- A small focus of 27Hz-centered beta oscillation was found at the confluence of ALIC, GP, and BNST, making it difficult to attribute to a single structure.

Physiological changes during provocation of an obsessive fear: As the microelectrode tip neared the ventral NAc target, the patient was handed a toothbrush and told to bring it to his face, and then to imagine it dirty while also imagining brushing his teeth with it. This test was performed for clinical purposes - to attempt neuronal action potential modulation correlated with his contamination obsession and confirm regional involvement of his disease, much like sensorimotor testing is used in movement disorders (Benabid et al. 2000). Robustly firing neurons were studied at two sites within NAc, 2mm from one another, and 4&6mm ventral to the dorsal border (Figure 2). In response to the provocation test, we made the following observations:

- At the more dorsal NAc site, firing rate of the measured neuron increased specifically during provocation of the compulsion. The amplitude of both the alpha and gamma oscillations increased with provocation (Figure 2, also illustrated in the supplemental videos at https://searchworks.stanford.edu/view/xf387wq3868). Unfortunately, the persistent post-provocation hand movement AP rate increase compared with resting seen during (though decreased compared with provocation) cannot be disentangled from ongoing obsessive feelings.
- Conversely, at the more ventral NAc site, firing rate of an isolated neuron as well as gamma amplitude decreased with provocation of the compulsion. At this location, there was significant correlation between 1s blocks of gamma oscillation amplitude and $\log_{10}$ spike rate during the pre-provocation period (Pearson's $R=0.56$, $p=4\times10^{-6}$), and not for the periods during or following provocation with the toothbrush. This effect was not seen at the more dorsal NAc site.

Discussion:

Downloaded from www.physiology.org/journal/jn at Auburn Univ Auburn (131.204.073.184) on April 25, 2019.

This NAc-specific $h\gamma_{35}$ oscillation implies a common physiological element amongst NAc microcircuits, which are known to be composed of medium spiny neurons (MSNs) and a variety of different classes of interneurons. The observation that obsession provocation induces opposite $h\gamma_{35}$–amplitude responses at different NAc sites implies that this common element is present across different NAc microcircuit types. In rats, a ~50Hz gamma oscillation ($r\gamma_{50}$) is present in NAc, and not the remainder of the striatum (Berke et al. 2004). Using pharmacological manipulation, it was shown that $r\gamma_{50}$ is specifically attributable to subthreshold fluctuations in the membrane potential of parvalbumin-positive GABAergic fast-spiking interneurons (FSIs) (Bracci et al. 2003). Furthermore, emerging work shows that output from these FSIs specifically constrains impulsive action (Pisansky et al. 2019). The rat $r\gamma_{50}$ may help us interpret the human $h\gamma_{35}$ if, as we hypothesize, both emerge from genetically homologous microcircuits that slightly diverged during evolution. Such human vs. rat homology is seen in 7 vs. 10Hz hippocampal oscillations (DeCoteau et al. 2007; Kahana et al. 1999). Computational modeling of ventral striatal networks shows that γ-oscillations emerge from the MSN-FSI interactions, and a small change in the timeconstant of GABAergic post-synapic current (such as might happen evolutionarily) could induce a shift from 50Hz to 35Hz in the emergent global oscillation of the microcircuit (Wu et al. 2017). Careful measurement showed that some NAc $r\gamma_{50}$ are coherent with select sites in prefrontal cortex, piriform cortex, and the hippocampus (Berke 2009). Assuming $h\gamma_{35}$-$r\gamma_{50}$ homology, $h\gamma_{35}$ coherence might reveal NAc interactions with these other brain areas in the human, which could be used as a tool for paired stimulation in neurosurgical intervention.

One might speculate that these oscillations actually facilitate information transfer between brain regions, beyond serving only as a signature of interaction, but that cannot be established from this case alone. Measurements from DBS macroelectrodes in the NAc found a similar ~10Hz oscillation during task engagement, but nothing consistent with the $h\gamma_{35}$ in the signal (Cohen et al. 2009a; b). This discrepancy might be explained if the microcircuit motif that generates a 35Hz isn't coherent across a large enough volume to be picked up by the DBS macroelectrode, which fits with the observation that the $h\gamma_{35}$ motif has conjugate changes in sites separated by just 2mm (Figure 2).

The finding that provocation of the patient's contamination obsession induced physiological changes in NAc is an initial step forward to better understand how obsessions are processed in the human brain. In isolation, differential action potential firing activity at different sites within NAc could be attributed to the capture of different neuron types within a functionally isotropic region. However, local field potentials reflect a property of the local ensemble of neurons and were also opposite in the magnitude of their shift with provocation, suggesting that the different electrophysiological responses we observed within the NAc reflect distinct microcircuits with different functions. Likely, our two conjugate responses to compulsive fear are from different types of microcircuits that share the $h\gamma_{35}$-FSI type, and may be related to different MSN types (e.g. D1 vs D2 dopamine receptors) (Graziane et al. 2016). The ~0.3-0.5mm scale of the arborization of these FSIs allows for the possibility of differential microcircuits across the 2mm distance where are differential observations were made (Koós and Tepper 1999). There are distinct MSN-based microcircuits in the rat NAc shell, which are topologically organized differentially by positive- and negative-motivational-valence (Reynolds and Berridge 2002). In light of this, differential NAc responses we observed may reveal conjugate motivational-valence

Downloaded from www.physiology.org/journal/jn at Auburn Univ Auburn (131.204.073.184) on April 25, 2019.

microcircuits, with obsession triggered increased firing rate and $h\gamma_{35}$-amplitude more dorsally, and the physiological converse 2mm beneath. During intraoperative stimulation testing of a DBS electrode advanced to target, our patient began smiling with an outwardly euphoric affect (Haq et al. 2011), while verbally stating this distressed him. This effect was not seen with more dorsal stimulation, and the 3mm-long electrode at target produced current density spread across both of the sites where the toothbrush task was performed. It may be that these contrasting effects were induced by simultaneous stimulation of multiple accumbens microcircuit types. Although NAc involvement in a brain circuit underlying OCD has been demonstrated with functional imaging (Figee et al. 2011) and inferred by clinical improvement with NAc-DBS (Fayad et al. 2016; Haq et al. 2011; Sturm et al. 2003), this case shows directly that provocation of an obsession is associated with changes in firing rate and LFP oscillatory power in human NAc.

Acknowledgments: We are grateful for the intraoperative support of the Bronte-Stewart laboratory and the helpful discussion with Drs. Dora Hermes, Kelly Foote, Joshua Berke, and Robert Malenka while interpreting the case and preparing the manuscript. This study was supported by the Van Wagenen Fellowship (KJM), funds from K12NS080223 (CHH), the Brain & Behavior Research Foundation (NRW and CHH), the Neurosurgery Research and Education Foundation (CHH), the John A. Blume Foundation (CHH), the William Randolph Hearst Foundation (CHH), the Stanford Neuroscience Institute's Neurochoice Initiative (CHH), and start-up funds from Stanford's Department of Neurosurgery (CHH).

Author contributions:

Conceived research: KJM, NRW, CHH
Performed experiments: All authors
Performed analyses and statistical comparisons: KJM
Prepared manuscript: KJM
Revised and approved manuscript: All authors

References:

Alonso P, Cuadras D, Gabriëls L, Denys D, Goodman W, Greenberg BD, Jimenez-Ponce F, Kuhn J, Lenartz D, and Mallet L. Deep brain stimulation for obsessive-compulsive disorder: a meta-analysis of treatment outcome and predictors of response. *PloS one* 10: e0133591, 2015.

American Psychiatric Association. *Diagnostic and statistical manual of mental disorders (DSM-5®)*. American Psychiatric Pub, 2013.

Baliki MN, Mansour A, Baria AT, Huang L, Berger SE, Fields HL, and Apkarian AV. Parceling human accumbens into putative core and shell dissociates encoding of values for reward and pain. *Journal of Neuroscience* 33: 16383-16393, 2013.

Benabid A-L, Krack P, Benazzouz A, Limousin P, Koudsie A, and Pollak P. Deep brain stimulation of the subthalamic nucleus for Parkinson's disease: methodologic aspects and clinical criteria. *Neurology* 55: S40-44, 2000.

Berke J. Fast oscillations in cortical - striatal networks switch frequency following rewarding events and stimulant drugs. *European Journal of Neuroscience* 30: 848-859, 2009.

Berke JD, Okatan M, Skurski J, and Eichenbaum HB. Oscillatory entrainment of striatal neurons in freely moving rats. *Neuron* 43: 883-896, 2004.

Bracci E, Centonze D, Bernardi G, and Calabresi P. Voltage - dependent membrane potential oscillations of rat striatal fast - spiking interneurons. *The Journal of physiology* 549: 121-130, 2003.

Downloaded from www.physiology.org/journal/jn at Auburn Univ Auburn (131.204.073.184) on April 25, 2019.

Cohen MX, Axmacher N, Lenartz D, Elger CE, Sturm V, and Schlaepfer TE. Good vibrations: cross-frequency coupling in the human nucleus accumbens during reward processing. *Journal of cognitive neuroscience* 21: 875-889, 2009a.
Cohen MX, Axmacher N, Lenartz D, Elger CE, Sturm V, and Schlaepfer TE. Nuclei accumbens phase synchrony predicts decision-making reversals following negative feedback. *Journal of Neuroscience* 29: 7591-7598, 2009b.
DeCoteau WE, Thorn C, Gibson DJ, Courtemanche R, Mitra P, Kubota Y, and Graybiel AM. Learning-related coordination of striatal and hippocampal theta rhythms during acquisition of a procedural maze task. *Proceedings of the National Academy of Sciences* 104: 5644-5649, 2007.
Fayad SM, Guzick AG, Reid AM, Mason DM, Bertone A, Foote KD, Okun MS, Goodman WK, and Ward HE. Six-nine year follow-up of deep brain stimulation for obsessive-compulsive disorder. *PloS one* 11: e0167875, 2016.
Figee M, Vink M, de Geus F, Vulink N, Veltman DJ, Westenberg H, and Denys D. Dysfunctional reward circuitry in obsessive-compulsive disorder. *Biological psychiatry* 69: 867-874, 2011.
Grant JE. Obsessive–compulsive disorder. *New England Journal of Medicine* 371: 646-653, 2014.
Graziane NM, Sun S, Wright WJ, Jang D, Liu Z, Huang YH, Nestler EJ, Wang YT, Schlüter OM, and Dong Y. Opposing mechanisms mediate morphine-and cocaine-induced generation of silent synapses. *Nature neuroscience* 19: 915, 2016.
Haq IU, Foote KD, Goodman WG, Wu SS, Sudhyadhom A, Ricciuti N, Siddiqui MS, Bowers D, Jacobson CE, and Ward H. Smile and laughter induction and intraoperative predictors of response to deep brain stimulation for obsessive-compulsive disorder. *Neuroimage* 54: S247-S255, 2011.
Kahana MJ, Sekuler R, Caplan JB, Kirschen M, and Madsen JR. Human theta oscillations exhibit task dependence during virtual maze navigation. *Nature* 399: 781, 1999.
Koós T, and Tepper JM. Inhibitory control of neostriatal projection neurons by GABAergic interneurons. *Nature neuroscience* 2: 467, 1999.
Mian MK, Campos M, Sheth SA, and Eskandar EN. Deep brain stimulation for obsessive-compulsive disorder: past, present, and future. *Neurosurgical focus* 29: E10, 2010.
Miller KJ, Sorensen LB, Ojemann JG, and den Nijs M. Power-Law Scaling in the Brain Surface Electric Potential. *PLOS Computational Biology* 5: e1000609, 2009.
Pisansky MT, Lefevre EM, Retzlaff CL, Trieu BH, and Rothwell PE. Nucleus Accumbens Fast-Spiking Interneurons Constrain Impulsive Action. *bioRxiv* 516609, 2019.
Reynolds SM, and Berridge KC. Positive and negative motivation in nucleus accumbens shell: bivalent rostrocaudal gradients for GABA-elicited eating, taste "liking"/"disliking" reactions, place preference/avoidance, and fear. *Journal of Neuroscience* 22: 7308-7320, 2002.
Romanelli P, Heit G, Hill BC, Kraus A, Hastie T, and Brontë-Stewart HM. Microelectrode recording revealing a somatotopic body map in the subthalamic nucleus in humans with Parkinson disease. *Journal of neurosurgery* 100: 611-618, 2004.
Sheth SA, Neal J, Tangherlini F, Mian MK, Gentil A, Cosgrove GR, Eskandar EN, and Dougherty DD. Limbic system surgery for treatment-refractory obsessive-compulsive disorder: a prospective long-term follow-up of 64 patients. *Journal of neurosurgery* 118: 491-497, 2013.
Sturm V, Lenartz D, Koulousakis A, Treuer H, Herholz K, Klein J, and Klosterkötter J. The nucleus accumbens: a target for deep brain stimulation in obsessive-compulsive-and anxiety-disorders. *Journal of chemical neuroanatomy* 26: 293, 2003.

Downloaded from www.physiology.org/journal/jn at Auburn Univ Auburn (131.204.073.184) on April 25, 2019.

Westphal CFO. Ueber Zwangsvorstellungen. *Berliner Klinische Wochenschrift* 46: 669-672, 1877.
Wu H, Miller KJ, Blumenfeld Z, Williams NR, Ravikumar VK, Lee KE, Kakusa B, Sacchet MD, Wintermark M, and Christoffel DJ. Closing the loop on impulsivity via nucleus accumbens delta-band activity in mice and man. *Proceedings of the National Academy of Sciences* 115: 192-197, 2018.
Wu Z, Guo A, and Fu X. Generation of low-gamma oscillations in a GABAergic network model of the striatum. *Neural Networks* 95: 72-90, 2017.

Figure captions:

Figure 1: A robust map of brain oscillations in the ventral capsule / ventral striatal region of the human brain. (A) Oscillations of different frequency are plainly visible in the raw voltage trace at three exemplar sites (+1, +8, +18mm above target). **(B)** Power spectral densities (PSDs) on log-log axes for the three sites in (A) show clear peaks in the theta (7Hz), alpha (9Hz), and gamma (35Hz) frequencies above a 1/f background shape (Miller et al. 2009). **(C)** PSDs were measured at 1mm intervals from the cannula to target location. Colored background lines show significant oscillations (green-7Hz/θ; blue-9Hz/α; orange-25Hz/β; red-35Hz/γ). **(D)** Anatomical plotting of oscillations revealed a plain topological correspondence between each oscillation and the underlying brain anatomy. Abbreviations: *sep* – septal nuclei / fornix; *LV* – lateral ventricle; *Cd* – caudate; *BN* – bed nucleus of the stria terminalis; *AC* – anterior commissure; *NAc* – nucleus accumbens; *DB* – diagonal band of Broca; *HTH* – hypothalamus; *ALIC* – anterior limb of internal capsule; *GP* – globus pallidus; *Put* – putamen.

Figure 2: Physiological changes during provocation of an obsessive fear that drives compulsive cleaning behavior. (A) Provocation was performed at two NAc sites (yellow/purple dots 4/6mm ventral to the dorsal NAc border). **(B)** After resting baseline, the patient was handed a toothbrush to bring to his face and was told "imagine brushing your teeth with this dirty toothbrush", followed by bringing his hand to his face without a toothbrush (see Supplemental video). **(C)** Action potential rate selectively increased during toothbrush-provocation at the yellow site. (‡p=1x10^{-6}/t=5.4; †p=0.05/t=-2.0, by unpaired t-test. Error bars show S.E.M. of 1s blocks). **(D)** PSDs reveal progressive power increase across all frequencies during the task at the yellow site. Inset axes show isolated alpha-range (8-10Hz, ‡p=2x10^{-6}/t=5.2) and gamma-range (31-39Hz, ‡p=7x10^{-7}/t=5.5) amplitudes. **(E)** Conversely, a neuron captured 2mm ventral (purple site) exhibited a significant decrease in spike rate (p=†8x10^{-3}/t=-2.7) and gamma-range amplitude (†p=0.04/t=-2.1; ‡p=4x10^{-6}/t=5.0) with provocation.

Downloaded from www.physiology.org/journal/jn at Auburn Univ Auburn (131.204.073.184) on April 25, 2019.

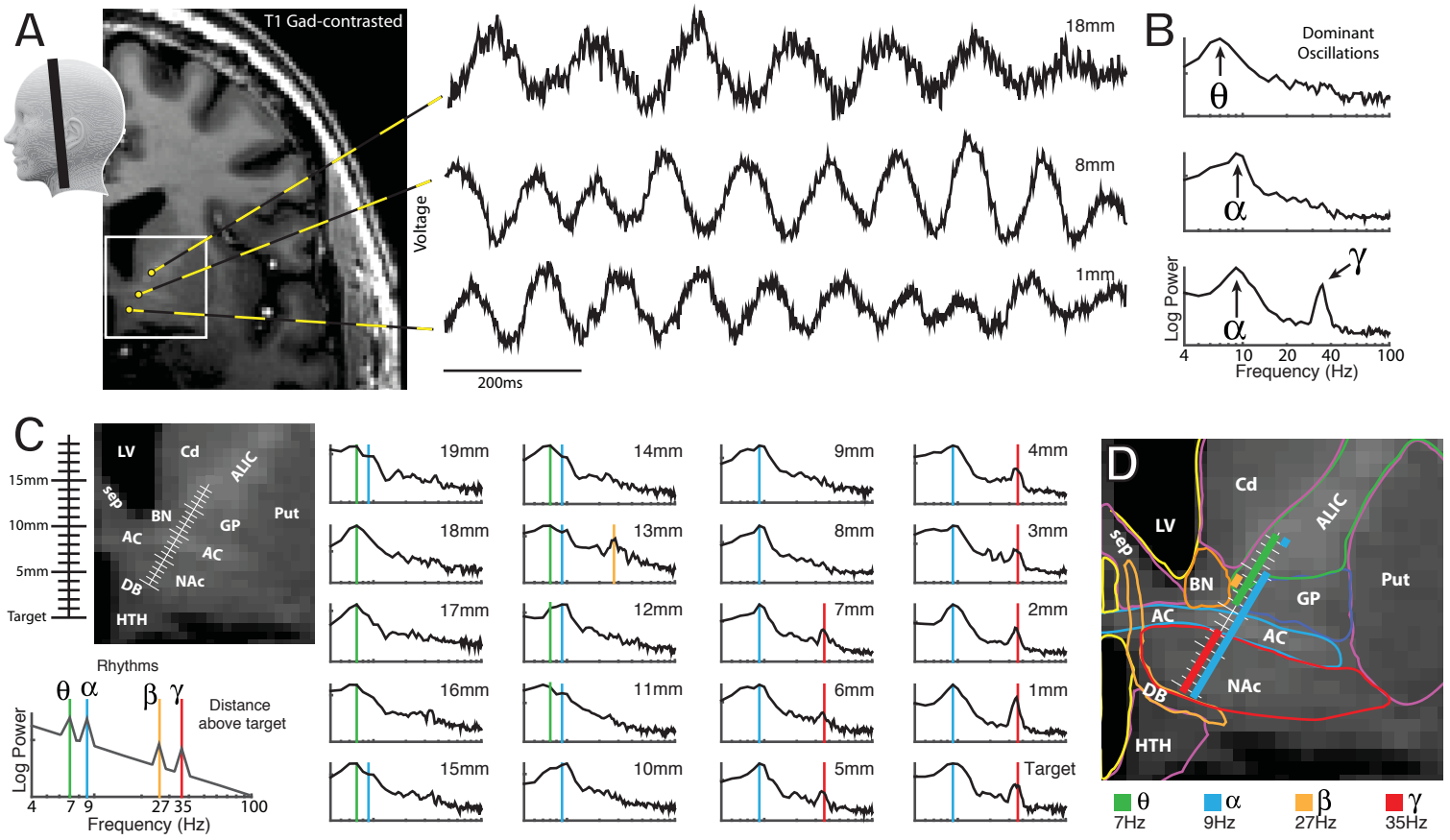

Downloaded from www.physiology.org/journal/jn at Auburn Univ Auburn (131.204.073.184) on April 25, 2019.

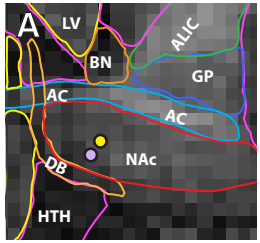

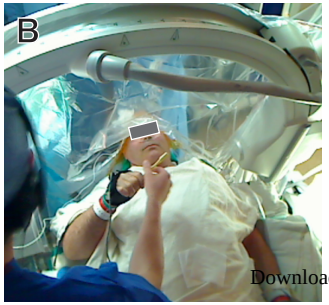

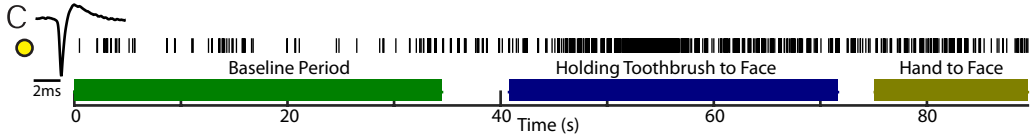

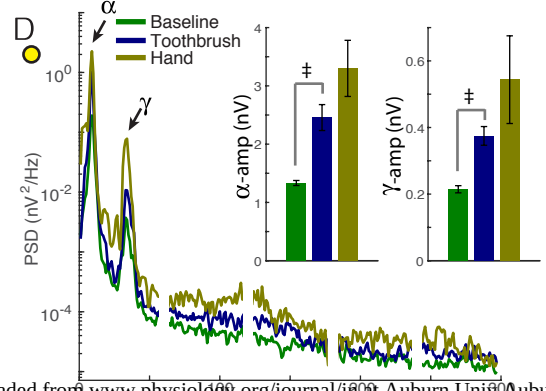

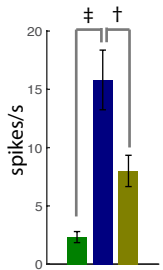

†: p≤0.05 ‡=p<10⁻⁵

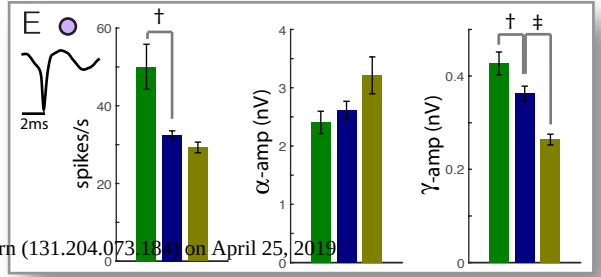

Downloaded from www.physiology.org/journal/jn at Auburn Univ Auburn (131.204.073.184) on April 25, 2019.